A Polarization-insensitive Dual-band Plasmonic Metamaterial Absorber for a Sensor Application

Yongqiang Kang

Shanxi Datong University - Yudong Campus: Shanxi Datong University https://orcid.org/0000-0001-6428-1807

Peng Gao

Qingdao University of Science and Technology

Hongmei Liu (hmliu@mail.xidian.edu.cn)

Institute of solid state physics, Shanxi Datong University, Datong, Shanxi 037009, China

Nano Express

Keywords: Palsmonics, Metamaterial, Absorber, FDTD

Posted Date: October 30th, 2020

DOI: https://doi.org/10.21203/rs.3.rs-99130/v1

Version of Record: A version of this preprint was published at Physica Scripta on March 26th, 2021. See the published version at https://doi.org/10.1088/1402-4896/abf007.

A polarization-insensitive dual-band plasmonic metamaterial absorber for a sensor application

Yongqiang Kang[1], Peng Gao[2], Hongmei Liu[1,3*]

[1]School of Physical Science and Electronics, Shanxi Datong University, Datong City 037009, People's Republic of China

[2]College of Mathematical and Physical Sciences, Qingdao University of Science and Technology, 266061, Qigndao, China.

[3]Institute of solid state physics, Shanxi Datong University, Datong, Shanxi 037009, China

* *Corresponding author: hmliu@mail.xidian.edu.cn*

Abstract

A polarization-insensitive dual-band plasmonic metamaterial absorber is proposed, which is constituted by merely the metal nano-cylinder and a continuous metallic ground separated by a middle dielectric layer. Two resonance peaks with over 99% absorbance derived from `the fundamental resonance and the surface lattice resonance are realized. In addition, we demonstrated that proposed dual-absorber retain nearly perfect absorbance for all polarization angles of both TE and TM modes on normal incidence. It is different from previous work that the dual-frequency response is obtained by combining two subunits of different sizes. Moreover, a first-order diffraction mode of grating predicted the resonance frequency of the proposed absorber. Importantly, the second absorption peak result from surface lattice resonance with narrow line-width has large sensitivity perform and high quality factor, which has significant potential in the application of biosensors and monitoring.

Keywords: Palsmonics, Metamaterial, Absorber, FDTD

1. Introduction

Recently, plasmonic metamaterials with their unordinary properties have obtained important progress due to their promising applications such as bio-sensor, absorbers, filters and photonic modulators [1-15]. Most of these applications greatly benefit from the unique properties of the sub-wavelength metallic structure supporting localized surface plasmonic resonance modes [16-27]. For these metamaterials devices, metamaterial absorbers have attracted much attention because of their excellent properties and wide applications [28-31].Generally, metamaterial absorber can be classified as broadband and narrowband type according to their different application requirements. Broadband absorbers are widely used in solar power harvesting and thermo emission. While narrowband absorbers are applied for photodetectors and sensor [9,11,14].

The first metamaterial absorber composed of metal-dielectric-metal was demonstrated by Landy in 2008 [32]. Since then, metamaterial absorbers have received extensive attention, and many absorbers have been proposed. However, most reported metamaterial absorbers have the shortcomings of single absorption bandwidth that are polarization-sensitive, which significantly hinder their practical applications [20,23] . It is necessary to design dual- or multiband metamaterial absorbers with polarization-insensitive. It is an effective method to obtain the dual-band or multiband response by combining the resonance of the superunit structure at several discrete frequencies [33-35]. For example, Feng *et al.* demonstrated dual-band and multiband infrared absorber by horizontally arranging

several subunits of different sizes into one unit cell [33]. Guo *et al.* presented ultra-broadband absorber by using four sub-wavelength resonators in the infrared region [34]. Zhang et al. reported a dual-band absorber by vertically stacking two distinct dielectrics [35]. However, these reported approaches face two challenging problems: large size unit problems and technical difficulties in manufacturing at higher frequencies such as terahertz, infrared, and visible region.

Herein, we demonstrate a polarization-insensitive dual-band plasmonic metamaterial absorber constituted by merely a metallic nano-cylinder and a continuous metallic ground separated by a middle dielectric layer. It is found that there are two distinct absorption bands whose peak absorption (about 98.6%) in the fundamental mode and peak absorption (99.9%) with surface lattice resonance. It is different from previous work that the dual-frequency response is obtained by combining two subunits of different sizes. The proposed dual-band absorber makes use of the overlap of the fundamental frequency resonance and the surface lattice resonance of the periodic structure formed by a single metal pattern, and thus making the proposed dual-band absorber quite easy to manufacture than previously reported structures. Importantly, the absorption peak results from surface lattice resonance not only has narrow line-width but also shows significant sensing characteristics for slight changes in the surrounding media. Furthermore, numerical simulations demonstrate the proposed absorber could retain high absorption level at large angles of polarization.

2. Structure and design

The proposed dual-band metamaterial absorber is shown in Fig. 1, which is consists of three layers. The top layer is a gold cylinder. The middle layer is the dielectric layer and the bottom layer is gold film. The gold cylinder-dielectric gold structure is abbreviated as GCDG. The structure is fabricated on a glass substrate. The gold cylinder had a radius (R) of 0.366 um, thickness of t=57 nm. The middle dielectric layer had a dielectric constant of 1.96 [23] and a thickness h=35 nm. The thickness of the ground layer gold film is L=0.1um, and the lattice constant is *P*=0.765 um. The dielectric constant of gold is from reference [33,34]. The finite difference time domain (FDTD) method is used to get the exact results. In the simulation, the periodic boundary condition is applied along the x and y direction, and perfectly matched layers are set along z-direction. The absorption of the structure is obtained by $A=1-T-R$, where transmission $T\approx 0$, when the thickness of metal plate (*L*=0.1um) is much larger than the skin depth. The perfect absorption can achieve as reflection close to zero (i.e. the equivalent impedance of metamaterial absorber structure matched to air).

3. Results and discussion

The reflectivity, transmission and absorption spectra of the GCDG are shown in Fig.2. It is clear that the reflectivity curve have two significant dips result from two distinct type resonances. The transmission *T* is zero owing to the presence of the metallic bottom layer, which blocks the transmission of the incident beam. Therefore, two discrete nearly perfect absorption peaks appear, the absorption of which are 98.6% (F_1=275.1THz) and 99.9% (F_2=440.1THz), respectively. The peak F_2 at 440.1THz

has the absorption line-width of 6THz, which is about one-fifth of the peak F_1 at the 275.1THz (the absorption line-width 30 nm). Furthermore, the quality factor (Q) is written as $Q = F / FWHM$, where F and $FWHM$ are the resonance frequency and the full width at half maximum, respectively [22,23]. The Q value of peak F_2 is about 73.4, which is 8.1 times of peak F_1. It is known that the narrow line-width and high Q value are promised for sensing performance.

The peak F_2 with narrower absorption line-width and higher Q come from the surface lattice resonance of the basic unit, while the peak F_1 arises from the fundamental resonance. To give an intuitive argument, we show the dependence of absorption spectra on the different lattice constant in Fig. 3. It can be found that the peak F_2 shift to less frequency with the increase of the lattice constant P, while the shift of peak F_1 is neglected. Therefore，the physical mechanism of peak F_2 is attributed to surface lattice resonance, which is distinct from previously reported sandwich structure with only EM resonance or interference mechanisms [24,25]. The surface lattice resonance can be predicted approximately by the first-order diffraction mode of grating [23]. The resonance frequency can by expressed as

$$f(\mathrm{i},\mathrm{j}) = \frac{\sqrt{i^2 + j^2}}{cbnP} \tag{1}$$

Where c is the light speed in air, b=0.88 is a numerical factor, n is the refractive index of the device surrounding, i and j are the grating diffraction orders, and P is the grating constant (or the unit period). The function relationship of the resonance frequency on the lattice period P is shown in Fig. 4. It can be seen that the resonance

frequency linearly rises with the lattice period P decreasing, which is same as shown in Fig.3. The theoretically predicted the resonance frequency indicated by pentagram agrees roughly with the result of simulation when the lattice period P varies from 0.765um to 0.825 um. The resonance frequency of surface lattice resonance in simulation results have a little deviation for the theoretical value of the one-order diffraction modes. This is because a surface lattice resonance involves the interplay of the dipole resonance and the first order diffraction mode [22,23].

To reveal the absorption mechanisms of the two resonance peak, the electromagnetic field distribution of the GCDG is shown in Fig. 5. Figures (a), (c), (e), (g) are the amplitude of electric field ($|\mathrm{E}|$) in the x-y plane, $|\mathrm{E}|$ in the x-z plane, z component of electric field (E_z), and magnetic field ($|H|$) at the resonance frequency F_1=275.1 THz, respectively. Electric field ($|\mathrm{E}|$) in the x-y plane, $|\mathrm{E}|$ in the x-z plane, z component of electric field (E_z), and magnetic field ($|H|$) at the frequency F_2=440.1THz are presented in Fig. 5 (b),(d), (f), (h), respectively. For the peak F_1 at 275.1THz, electric field mainly concentrates in the cavity between the metallic cylinder and dielectric, as shown in Figs. 5(a) and 5(c). A large number of positive and negative charges accumulated and form a strong electric dipole resonance, as shown in Fig. (e). The magnetic field distribution is mainly gathered in the bottom edges of the metallic cylinder, as shown in Fig. 5(g). As a result, peak F_1 result from the fundamental electric and magnetic dipole resonance.

Whereas, at the resonance frequency F_2=440.1 THz, the electromagnetic field distribution features the surface lattice resonance [23]. It is seen in Figs 5(b) and 5(d)

that the electric field distributions mainly concentrate symmetrically on the top surface edges of the cylinder. Figure 5(f) shows the opposite surface charges are accumulated on the edges of the metallic cylinder, which has similar distribution characteristics with the amplitude of electric field of the fig. 5(b). The magnetic field is distributed in the top cylinder edge and the middle dielectric layer, as show in fig 5 (h). Thus, the peak F_2 is attributed to lattice resonance [1, 23]. Therefore, we proposed a new approach to obtain dual-band absorber by combining two different resonance modes in a single pattern structure.

In lots of situations, it is desirable to design a polarization insensitive absorber [23, 24]. Figure 6(a) and (b) show the dependence of the GCDG on the polarization angle for the TE and TM modes, respectively. It is found that the location of absorption peaks and absorbance remained unchanged as the polarization angle change from 0 to 90 degree at normal incidence. It is easily understood because of the high degree of symmetry for the metallic cylinder in Fig 1.

Since the first absorption peak has a high Q value, it is promising for sensing application [22,27]. For verification, Fig 7(a) shows the dependence of the absorption spectrum when the surrounding refractive index (RI) from n=1.0 (air) to1.1 with the interval of 0.02. From Fig. 7(a), we can find that peak F_2 is red-shift, while the peak F_1 changes weakly with the increase of the RI.

The functional relationship between the resonance peak F_2 and the RI (n) is shown in Fig. 7(b). It is shown that resonant peak redshift linearly with the increasing the RI of surrounding. Additionally, the absorption bandwidth and absorption are

almost unchanged due to the impedance of the proposed absorber matched to the free space. To evaluate the sensing performance of the proposed absorber, the sensitivity (S) and the figure of merit (FOM) are defined as follows [22,23]:

$$S = \Delta F / \Delta n,\ FOM = S / FWHM \tag{6}$$

where ΔF and Δn are the changes of the resonance frequency and RI, respectively. From Eq.(6), the sensitivity and FOM of the resoanance peak F_2 are 160 THz/RIU and 27 , respectively. This is larger than the value based on the gap resonance mode. More importantly, the proposed absorption device has a better sensitivity, which is over the existing reported [37, 38].

4. **Conclusion**

A simple design of polarization-insensitive dual-band plasmonic metamaterial absorber composed by only a gold nano-cylinder and a continuous gold ground separated by a middle dielectric layer is reported. Two distinct absorption peaks derived from `the fundamental resonance and the surface lattice resonance with over 99% absorbance are presented. Moreover, a first-order diffraction mode of the grating predicted the resonance frequency of the GCDG absorber. In addition, proposed dual-band absorber is insensitivity for all polarization angles of both TE and TM modes on normal incidence. Importantly, the absorption peak result from surface lattice resonance has high Q and a large sensitivity, which has significant potential in the application of biosensors.

Acknowledgements

This research was financially supported by National Science Foundation for

China (Grant NO. 11874245) and Shanxi Provincial Natural Science Foundation (Grant NO. 201801D121071, 201701D221096) and Scientific and Technological Innovation Project of Colleges in Shanxi Province (Grant NO. 2019L0741).

Reference

[1]J. A. Schuller, E. S. Barnard, W. S. Cai, Y. C. Jun, J. S. White, and M. L. Brongersma, (2010) Plasmonics for extreme light concentration and manipulation. Nature Materials 9:193–204

[2]J. W. Mu, L. Chen, X. Li, W. P. Huang, L. C. Kimerling, and J. Michel (2013) Hybrid nano ridge plasmonic polaritons waveguides. Appl. Phys. Lett. 103:131107

[3] H. Lu, X. Liu, D. Mao, and G. Wang (2012) Plasmonic nanosensor based on Fano resonance in waveguide-coupled resonators. Opt. Lett. 37: 3780–3782

[4]Y. K. Gong, X. Liu, K. Li, J. Huang, J. J. Martinez, D. R. Whippey, and N. Copner (2013) Coherent emission of light using stacked gratings. Phys. Rev. B 87: 205121

[5] C. H¨agglund and S. P. Apell (2012) Plasmonic near-field absorbers for ultrathin solar cells. J. Phys. Chem. Lett. 3: 1275–1285

[6] J. W. Mu, X. Li, and W. P. Huang (2010) Compact Bragg grating with embedded metallic nano-structures. Opt. Express 18, 15893–15900

[7] J. Y. Ou, E. Plum, L. Jiang, and N. I. Zheludev (2011) Reconfigurable photonic metamaterials. Nano Lett. 11: 2142–2144

[8]G. Wang, H. Lu, X. Liu, D. Mao, and L. Duan (2011) Tunable multi-channel wavelength demultiplexer based on MIM plasmonic nanodisk resonators at

telecommunication regime. Opt. Express 19: 3513–3518

[9] I. M. Pryce, Y. A. Kelaita, K. Aydin, and H. A. Atwater (2011) Compliant metamaterials for resonantly enhanced infrared absorption spectroscopy and refractive index sensing. ACS Nano 5: 8167–8174

[10] H. T. Chen, J. F. O'Hara, A. K. Azad, A. J. Taylor, R. D. Averitt, D. B. Shrekenhamer, and W. J. Padilla (2008) Experimental demonstration of frequency-agile terahertz metamaterials. Nature Photon. 2: 295–298

[11]A. E. Cetin and H. Altug (2012) Fano resonant ring/disk plasmonic nanocavities on conducting substrates for advanced biosensing. ACS Nano 6: 9989–9995

[12] J. Zi, Q. Xu, Q. Wang, C. Tian, Y. Li, X. Zhang, J. Han, and W. Zhang (2018) Antireflection-assisted all-dielectric terahertz metamaterial polarization converter. Appl. Phys. Lett., 113: 101104

[13] G. Kajtar, M. Kafesaki, E. N. Economou, and C. M. Soukoulis (2016) Theoretical model of homogeneous metal-insulator-metal perfect multi-band absorbers for the visible spectrum. J. Phys. D, 49: 055104

[14] D. Wu, R. F. Li, Y. M., Liu, Z. Y. Yu, L. Chen, C. Liu, R. Ma, and H. Ye (2017) Ultra-narrow band perfect absorber and its application as plasmonic sensor in the visible region. Nanoscale Research Letters 12:427

[15] Y. He, Q. Wu, and S. Yan (2019) Multi-band terahertz absorber at 0.1-1 THz frequency based on ultra-thin metamaterial. Plasmonics 14: 1303-1310

[16] J. Wu, F. Zhang, Q. Li, J. Chen, Q. Feng, and L. Wu (2020) Infrared

five-band polarization insensitive absorber with high absorptivity based on single complex resonator. Opt. Commun., 456:124575

[17] J. Zhang, J. Tian, L. Li (2018) A dual-band tunable metamaterial nearunity absorber composed of periodic cross and disk graphene arrays. IEEE Photon. J. 10:4800512

[18] J. Song, L. Wang, M. Li, and J. Dong (2018) A dual-band metamaterial absorber with adjacent absorption peaks. J. Phys. D, 51: 385105

[19] C. Y. Luo, D. Li, Qin, L. J. Yue, P. Gao, J.Q. Yao, F. R. Ling (2015) Design of a tunable multiband terahertz waves absorber. Journal of Alloys & Compounds 652:18-24

[20] H. M., Liu, Y.Q, Kang, T. Meng, C. Tian, & G. Wei (2020) High photon absorptivity of quantum dot infrared photodetectors achieved by the surface plasmon effect of metal nanohole array. Nanoscale Research Letters, 15: 98

[21] J. Zhang, J. Tian, S. Xiao, L. Li (2020) Methodology for High Purity Broadband Near-Unity THz Linear Polarization Converter and its Switching Characteristics. IEEE Access, 8(1):46505-46517

[22] X.Y. Lu, R. Wan and T. Zhang (2015) Metal-dielectric-metal based narrow band absorber for sensing applications. Optics Express 23: 29842

[23] B.X. Wang, W. Q. Huang , and L. L. Wang (2017) Ultra-narrow terahertz perfect light absorber based on surface lattice resonance of a sandwich resonator for sensing applications. RSC Advances 68:42956-42963

[24] S. Ji, C. Jiang, J. Zhao, X. Zhang, & Q. He (2019) Design of a

polarization-insensitive triple-band metamaterial absorber. Optics Communications 432:65-70

[25] X. Shen, Y. Yang, Y. Zang, J. Gu, J. Han, & W. Zhang, et al. (2012) Triple-band terahertz metamaterial absorber: design, experiment, and physical interpretation. Applied Physics Letters 101(15): 207402-445

[26] H. T. Chen, H. Yang, R. Singh, J. F. O'Hara, A. K. Azad, & S. A. Trugman, et al. (2010) Tuning the resonance in high temperature superconducting terahertz metamaterials. Physical Review Letters 105(24): 247402

[27] I. M. Pryce, Y. A. Kelaita, K. Aydin, & H. A. Atwater (2011) Compliant metamaterials for resonantly enhanced infrared absorption spectroscopy and refractive index sensing. ACS Nano, *5*(10): 8167-8174

[28] J. Hao, L. Zhou, & M. Qiu (2011) Nearly total absorption of light and heat generation by plasmonic metamaterials. Physical Review B Condensed Matter, 83(16):5919-5926

[29] H. Gao, C. Gu, Z. Y. Zheng, S. J. Chen, & H. Y. Hao (2014) Nearly perfect absorption in a single-layer metallic grating with rectangular grooves on its front surface. Applied Physics B 117(3): 875-883

[30] P. V. Tuong, J. W. Park, V. D. Lam, W. H. Jang , S. A. Nikitov , & Y. P. Lee (2013) Dielectric and ohmic losses in perfectly absorbing metamaterials. Optics Communications. 295: 17-20

[31] S. J. Li, P. X. Wu, H. X. Xu, Y. L. Zhou, X. Y. Gao, J. F. Han, H. H.Yang, Z. Zhang (2018) Ultra-wideband and polarization-insensitive perfect absorber using

multilayer metamaterials, lumped resistors, and strong coupling effects. Nanoscale Research Letters 13: 386

[32] N. I. Landy, S. Sajuyigbe, J. J. Mock, D. R. Smith, & W. J. Padilla (2008) A perfect metamaterial absorber. Physical Review Letters 100(20): 207402

[33] R. Feng, J. Qiu, L. H. Liu (2014) Parallel LC circuit model for multi-band absorption and preliminary design of radiative cooling. Optics Express 22: 1713-1724

[34] W. L. Guo , Y. Liu , and T. Han (2016) Ultra-broadband infrared metasurface absorber. Optics Express 18:20586-20592

[35] N. Zhang, P. Zhou, D. Cheng, X. Weng, & L. Deng (2013) Dual-band absorption of mid-infrared metamaterial absorber based on distinct dielectric spacing layers. Optics Letters 38(7): 1125-7

[36] D. Cheng, J. Xie, H. Zhang, C. Wang, & L. Deng (2012) Pantoscopic and polarization-insensitive perfect absorbers in the middle infrared spectrum. JOSAB 29(6): 1503-1510

[37] Q. Xie, G.X. Dong,B.X. Wang,and W.Q. Huang（2018）High-Q fano resonance in terahertz frequency based on an asymmetric metamaterial resonator. Nanoscale Res. 13:294

[38] R. Yahiaoui, A.C. Strikwerda, and P.U. Jepsen (2016) Terahertz palsmonic structure with enhanced sensing capabilities. IEEE Sensors 16: 2484

Figure Captions

Fig.1. (color online) Schematic of the proposed dual-band absorber. The yellow regions are gold, and light blue region is dielectric. R and t represent respectively, the radius and height of cylinder. h and L denote the thickness of the dielectric layer and the gold film. P is the lattice constant.

Fig.2. (color online) Refection, transmission and absorption spectra of the dual-band absorber. Parameters: P=0.765um, R=0.365um, h=35nm, L=0.1um.

Fig.3. (color online) Dependence of absorption spectrum on the changes of lattice period P of the dual-band absorber. Parameters: R=0.365um, h=35nm, L=0.1um.

Fig.4. (color online) comparison between the predicted resonance frequency and results obtained from the full-wave simulation for different lattice period P. Parameters: R=0.365um, h=35nm, L=0.1um, t=57nm.

Fig.5. (color online) (a), (c), (e),and (g) electricfield and magnetic field distribution at resonance frequency F1=275.1THz; (b),(d), (f), and (h) electricfield and magnetic field distribution at resonance frequency F2=440.1THz. Parameters: P=0.765um, R=0.365um, h=35nm, L=0.1um.

Fig.6. (color online) Simulated absorbance for different polarization angle: (a) TE,(b) TM. Parameters: P=0.765um, R=0.365um, h=35nm, L=0.1um.

Fig.7. (color online) (a) Dependence of the absorption spectrum on the changes of refractive index (n) of the surrounding; (b) Relationship between the resonance frequency and refractive index. Parameters: P=0.765um, R=0.365um, h=35nm, L=0.1um.

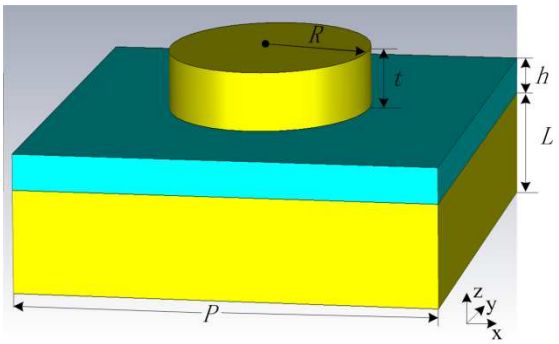

Fig. 1.(color online) Schematic of the proposed dual-band absorber. The yellow regions are gold, and light blue region is dielectric. R and t represent respectively, the radius and height of cylinder. h and L denote the thickness of the dielectric layer and the gold film. P is the lattice constant.

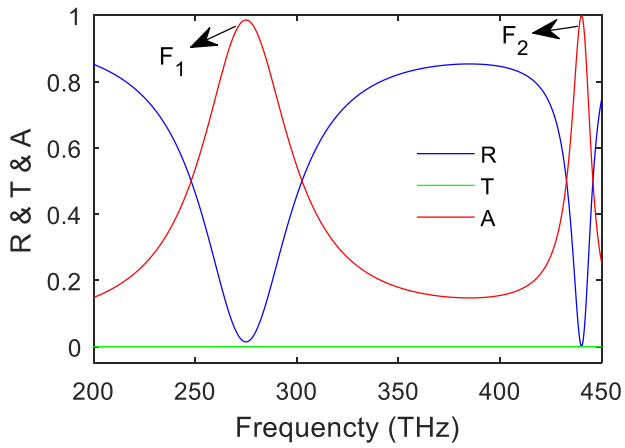

Fig.2. (color online) Refection, transmission and absorption spectra of the dual-band absorber. Parameters: P=0.765um, R=0.365um, h=35nm, L=0.1um.

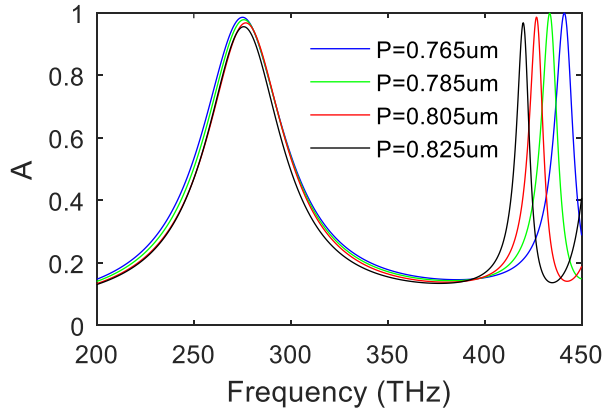

Fig.3. (color online) Dependence of absorption spectrum on the changes of lattice period P of the dual-band absorber. Parameters: R=0.365um, h=35nm, L=0.1um.

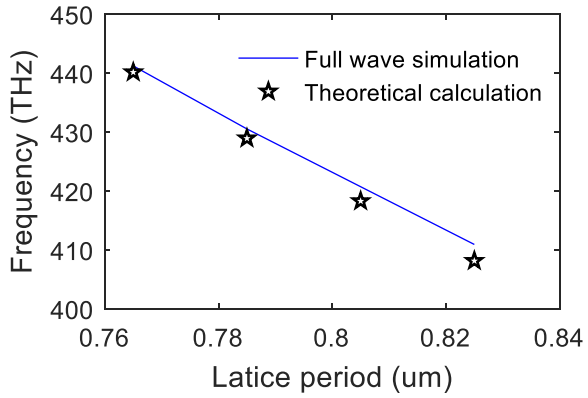

Fig.4. (color online) comparison between the predicted resonance frequency and results obtained from the full-wave simulation for different lattice period *P*. Parameters: R=0.365um, h=35nm, L=0.1um, t=57nm.

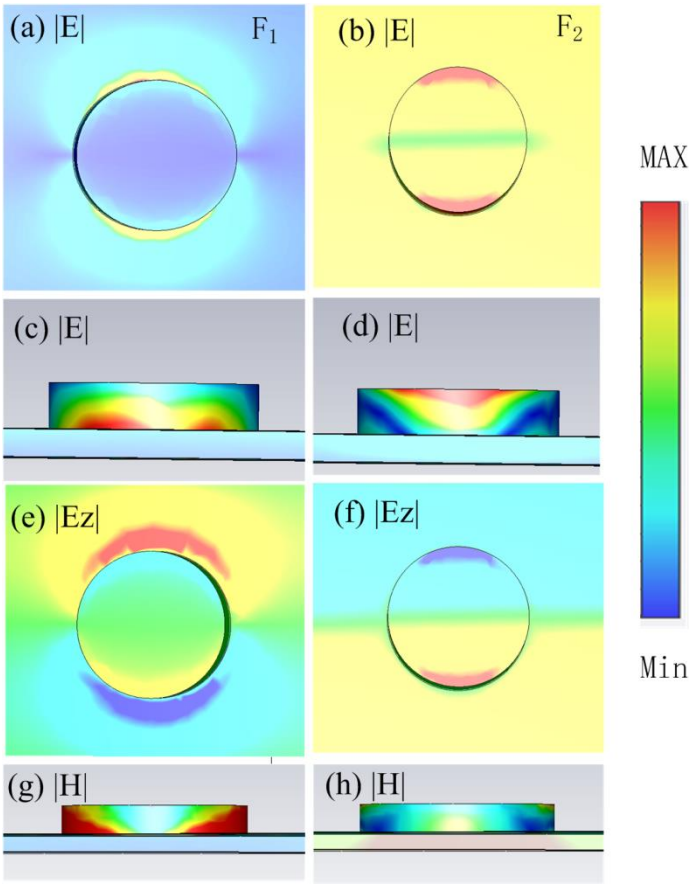

Fig.5. (color online) (a), (c), (e),and (g) electricfield and magnetic field distribution at resonance frequency F_1=275.1THz; (b),(d), (f), and (h) electricfield and magnetic field distribution at resonance frequency F_2=440.1THz. Parameters: P=0.765um, R=0.365um, h=35nm, L=0.1um.

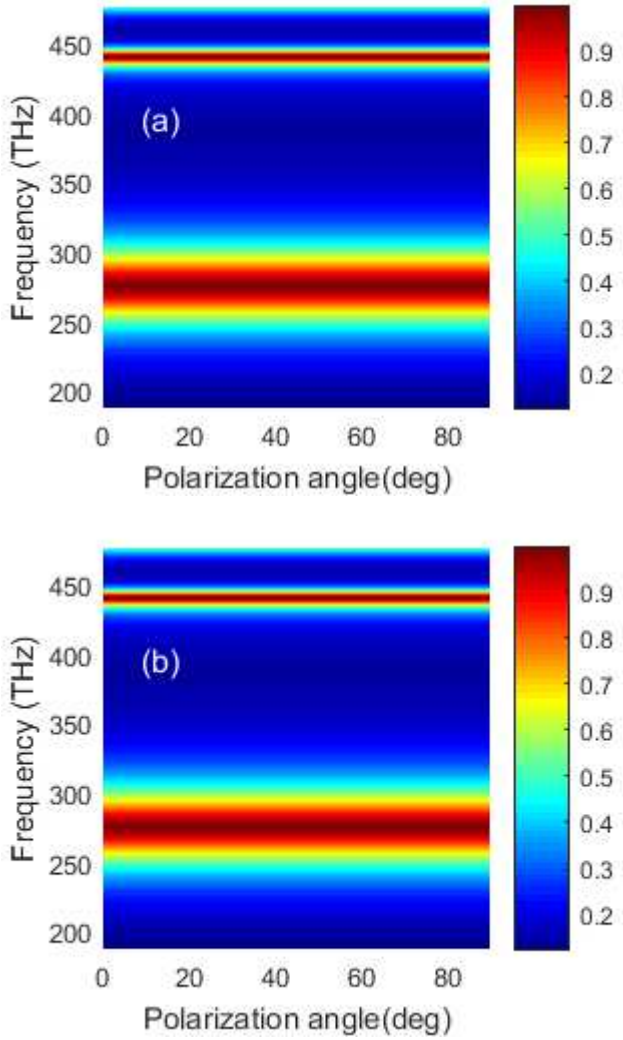

Fig.6. (color online) Simulated absorbance for different polarization angle: (a) TE,(b) TM. Parameters: P=0.765um, R=0.365um, h=35nm, L=0.1um.

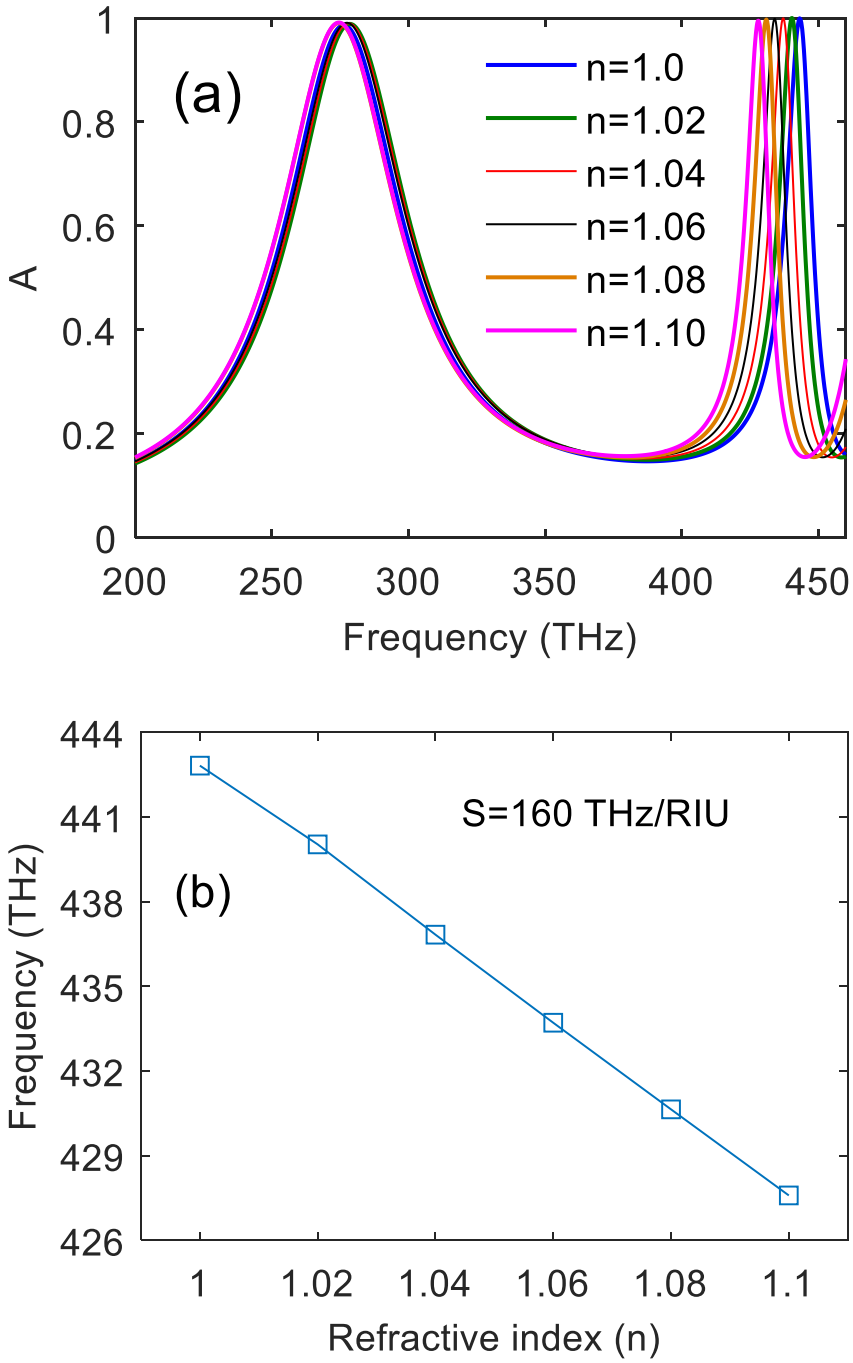

Fig.7. (color online) (a) Dependence of the absorption spectrum on the changes of refractive index (n) of the surrounding; (b) Relationship between the resonance frequency and refractive index. Parameters: P=0.765um, R=0.365um, h=35nm, L=0.1um.

Figures

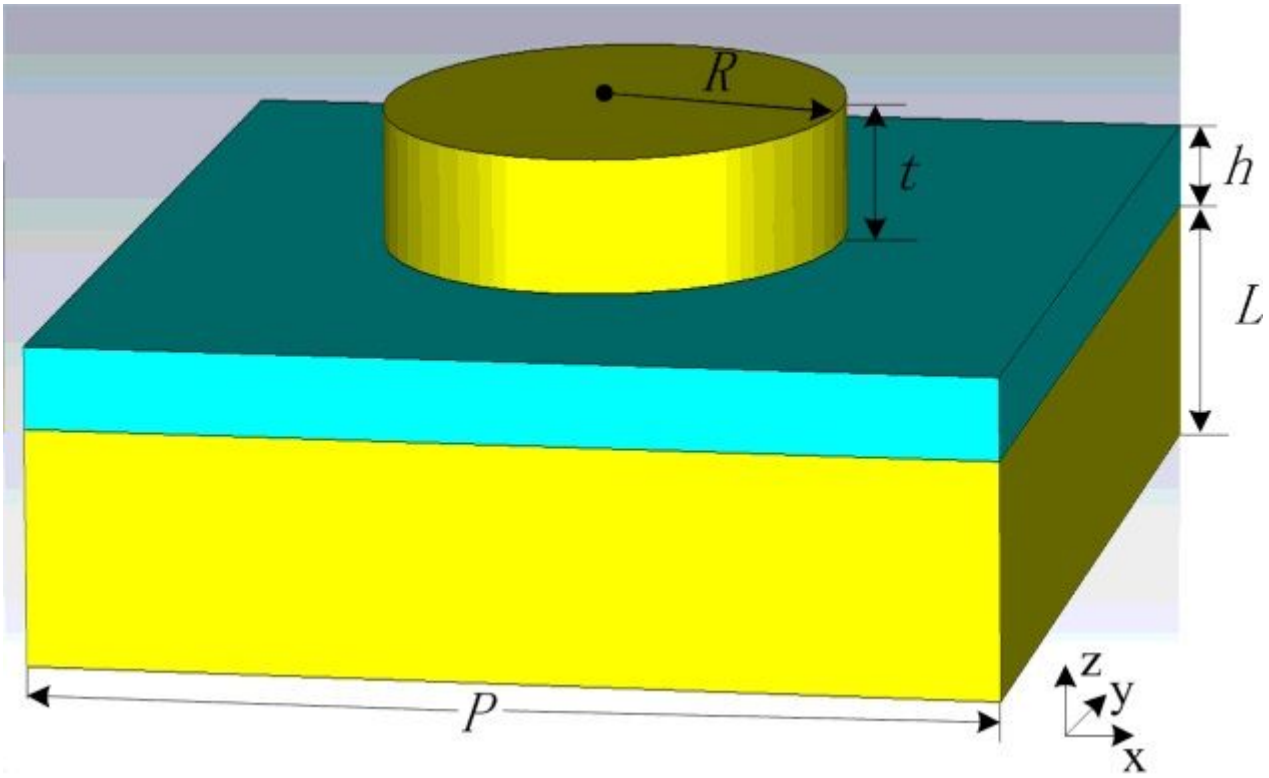

Figure 1

(color online) Schematic of the proposed dual-band absorber. The yellow regions are gold, and light blue region is dielectric. R and t represent respectively, the radius and height of cylinder. h and L denote the thickness of the dielectric layer and the gold film. P is the lattice constant.

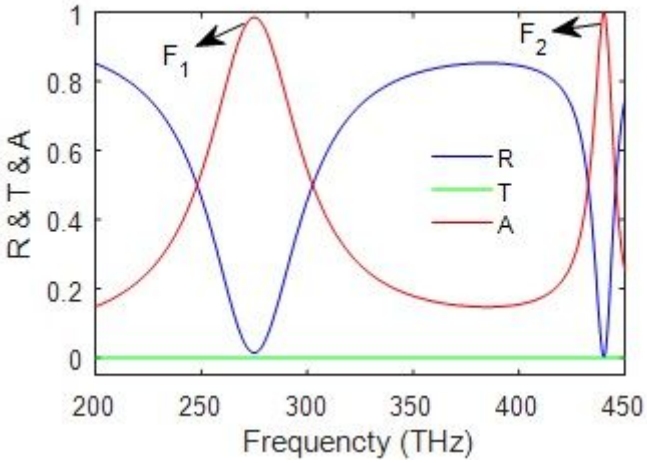

Figure 2

(color online) Refection, transmission and absorption spectra of the dual-band absorber. Parameters: P=0.765um, R=0.365um, h=35nm, L=0.1um.

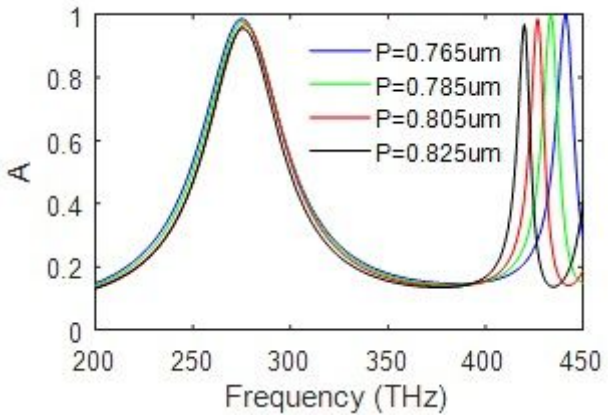

Figure 3

(color online) Dependence of absorption spectrum on the changes of lattice period P of the dual-band absorber. Parameters: R=0.365um, h=35nm, L=0.1um.

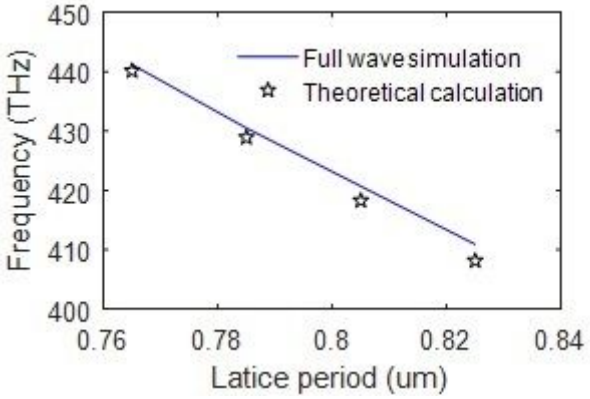

Figure 4

(color online) comparison between the predicted resonance frequency and results obtained from the full-wave simulation for different lattice period P. Parameters: R=0.365um, h=35nm, L=0.1um, t=57nm.

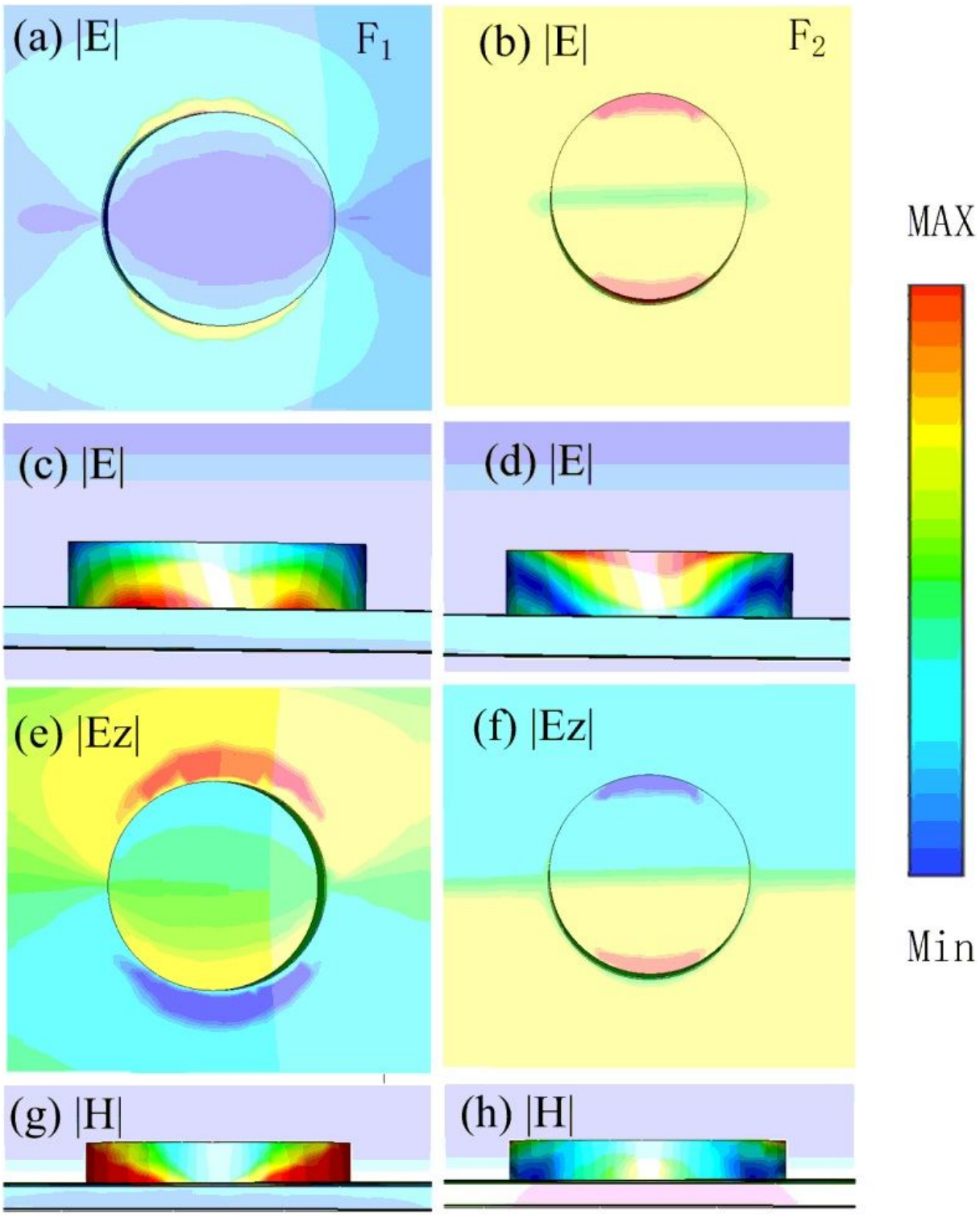

Figure 5

(color online) (a), (c), (e),and (g) electricfield and magnetic field distribution at resonance frequency F1=275.1THz; (b),(d), (f), and (h) electricfield and magnetic field distribution at resonance frequency F2=440.1THz. Parameters: P=0.765um, R=0.365um, h=35nm, L=0.1um.

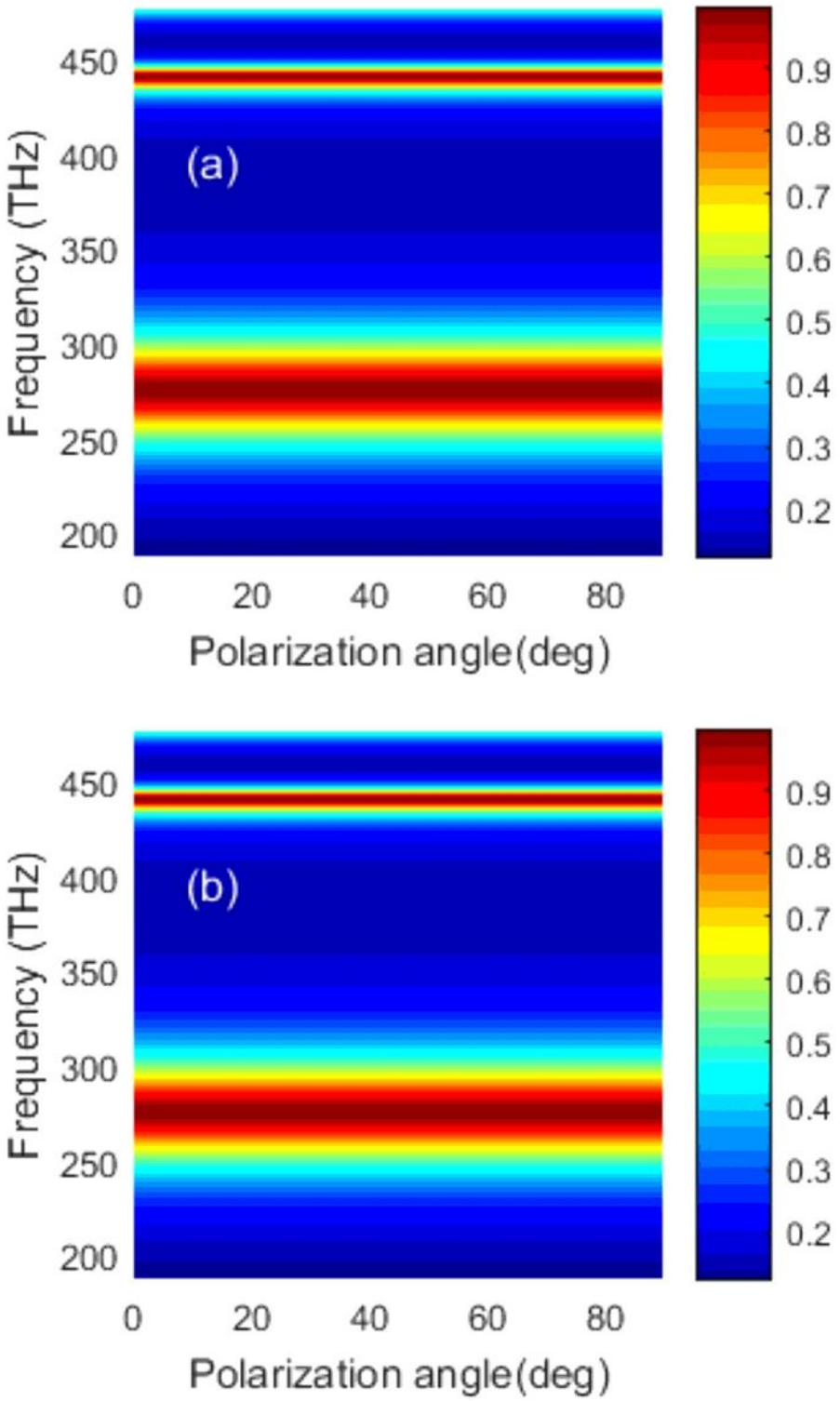

Figure 6

(color online) Simulated absorbance for different polarization angle: (a) TE,(b) TM. Parameters: P=0.765um, R=0.365um, h=35nm, L=0.1um.

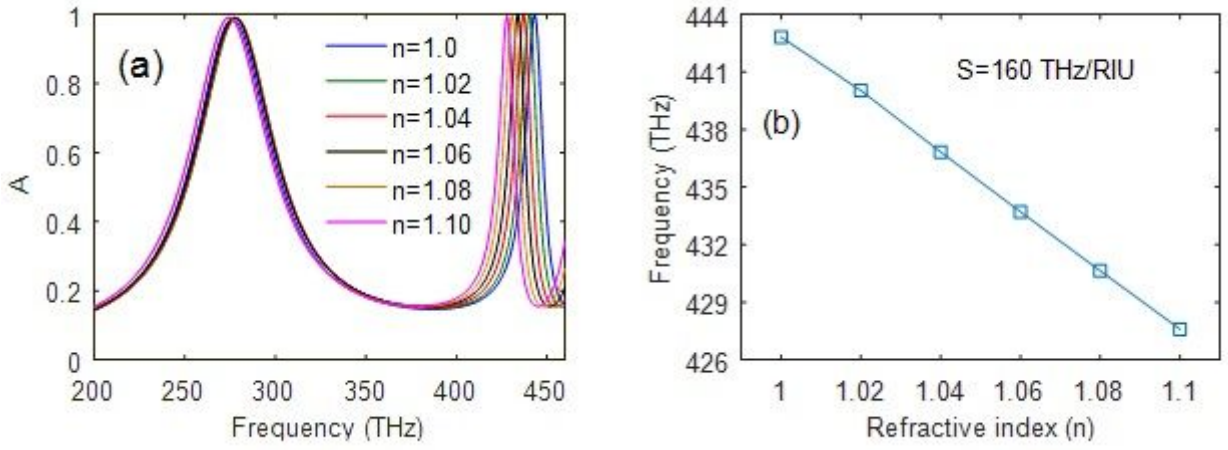

Figure 7

(color online) (a) Dependence of the absorption spectrum on the changes of refractive index (n) of the surrounding; (b) Relationship between the resonance frequency and refractive index. Parameters: P=0.765um, R=0.365um, h=35nm, L=0.1um.